

ASSESSMENT OF THE MELCOR AND RELAP5-3D CODE FOR CONDENSATION IN THE PRESENCE OF NONCONDENSABLE GAS

Wen Fu¹, Dhongik Yoon², and Michael L. Corradini²

¹: Institute of Nuclear and New Energy Technology, Tsinghua University, Beijing 100084, China

²: Department of Engineering Physics, University of Wisconsin-Madison, 1500 Engineering Drive, Madison, WI 53706, USA

fuw12@mails.tsinghua.edu.cn; dsyoon@wisc.edu; corradini@engr.wisc.edu

Mark H. Anderson²

²: Department of Engineering Physics, University of Wisconsin-Madison, 1500 Engineering Drive, Madison, WI 53706, USA

manderson@engr.wisc.edu

ABSTRACT

Condensation of steam plays an important part in removing heat from the reactor containment. The process is complicated by the presence of noncondensable gases in the containment. The condensation models considering the presence of noncondensable gases of RELAP5-3D code, MELCOR code and the generalized diffusion layer model were examined via simulation of the scaled AP600 atmospheric containment tests at UW-Madison. Examining the basic models and assumptions each code uses for the condensation mechanism, it was found that MELCOR and RELAP-3D use different models for calculating condensation mass flux. After examination of the models for each system code, we found that the condensation model in RELAP-3D needs to be corrected to properly account for the presence of noncondensable gases. The MELCOR simulation results showed good agreement with the experimental data. Also the effect of nodalizations on condensation heat transfer predictions was studied.

KEYWORDS

Condensation model; Noncondensable gas; RELAP5-3D; MELCOR; Diffusion layer model

1. INTRODUCTION

Upon a postulated nuclear plant accident where high pressure and high temperature water escapes into the containment in the form of superheated steam, the pressure and temperature increase in containment. Condensation heat transfer is an important physical process that helps keep the temperature and pressure in containment within the design limits, and ensures the containment integrity. However, the presence of noncondensable gases in the containment complicates and often hinders the process of heat transfer. Thus, an accurate model for condensation with noncondensable gases is, therefore, essential.

A schematic view of condensation with noncondensable gas on a vertical surface is shown in Fig. 1. The rate of condensation and therefore the rate of heat transfer out of the system depend on the degree of wall subcooling relative to the interface temperature, T_i , at the condensate surface. Noncondensable gases tend to accumulate at the interface, because the interface is impermeable to the noncondensable gases and steam condenses to water at the interface. This leads to the vapor partial pressure and temperature at the interface to be lower than those in the bulk region, as shown in Fig. 1. The noncondensable gas acts as

resistance to mass transfer and reduces temperature difference ($T_i - T_w$), thereby reducing heat flux through the liquid film.

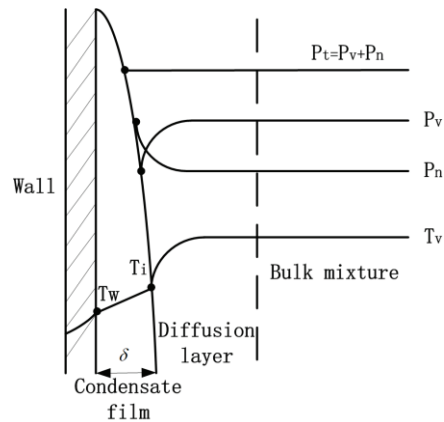


Figure 1. Condensation Schematic in the Presence of Noncondensable Gas.

Several researchers have performed experiments and investigated the effect of noncondensable gases on condensation heat transfer. The best known experimental data applied to accident safety analysis of containments were obtained by Uchida [1] and Tagami [2]. They investigated condensation heat transfer in a steel containment ($\sim 45\text{m}^3$) at low pressures (0.1 to 0.5 MPa) in the presence of noncondensable gases (varying amounts of nitrogen, argon and air). Their results indicated that the condensation heat transfer coefficients decreased with decreasing the mass fraction of noncondensable gas. Dehbi [3] tested the condensation heat transfer on the cooling tube in the closed cylinder chamber. The pressure in this experiment ranged from 1.5 to 4.5 atm. This experiment was performed to determine the effects of noncondensable fraction, length, wall temperature subcooling and total gas pressure. It was concluded that the heat transfer coefficient decreased significantly with increasing air mass fraction and decreasing total gas pressure. Anderson [4] investigated steam condensation onto the internal surface of a scaled AP600 containment surface with similar aspect ratios to the actual AP600. The effects of the bulk temperatures, the noncondensable gas mass fraction, the cold wall surface temperature, the pressure, noncondensable composition, and the inclination of the condensing surface were studied.

Theoretical research has also been conducted. Colburn and Hougen [5] first introduced the concept of a noncondensable gas boundary layer in the condensation of vapor-air mixtures. Their work assumed that the overall heat transfer between the cooling wall and the vapor-air mixture can be broken down to conductance of the liquid film and heat transfer of gas layer. The heat transfer through the gas layer includes sensible and latent heat transfer. Corradini [6] derived a condensation model for forced and natural convection by extending the Reynolds-Colburn analogy for heat and momentum transfer to mass and momentum transfer. Since the enhancement of mass transfer due to a suction effect is not addressed by the analogy formulation, Corradini used correction factors according to the methodology outlined by Bird [7]. This model was in reasonable agreement with the steady-state data of Uchida [1] and Tagami [2]. Subsequently Kim and Corradini [8] extended the Corradini's original model to a two-dimensional condensation model using a $k-\epsilon$ model to investigate the effect of two-dimensional flow. Based on the mass transfer equations and boundary conditions for condensation with noncondensable gases, Peterson [9] derived an effective "condensation thermal conductivity". With this simple parameter, combined sensible and condensation heat transfer can be predicted using the standard forms for heat transfer correlations. Peterson's model can be improved further by considering the effects of fog formation, suction, and condensate film waviness. Brouwers [10] introduced fog correction factors for both sensible

and latent heat transfer. Based on Peterson's approach, Herranz [11] extended the model to deal with large gas-wall temperature differences, high mass fluxes, and the wavy structure of the condensate. This model has been validated against the database of Anderson [4] and comparisons to Dehbi's [3] database have also been conducted. Peterson [12] developed an analysis of the mass transport with multiple noncondensable species, identifying a method to calculate an effective mass diffusion coefficient that can be used with the diffusion layer model. Liao [13] developed a generalized diffusion layer model for condensation of vapor from vapor/noncondensable gas mixtures by formulating the mass diffusion on a mass basis. Comparisons with a variety of experimental data show that this generalized diffusion layer model can better predict the data than molar-based diffusion layer models. Kim [14] proposed a theoretical model to estimate the condensation heat transfer at high pressure using the heat and mass transfer analogy. The comparison results confirm that the heat and mass transfer analogy can be applied to evaluate the condensation heat and mass transfer under high pressure conditions.

Two widely used system codes in the nuclear industry are RELAP5 and MELCOR. Both have condensation models considering the presence of noncondensable gases. The RELAP5 code is primarily used to analyze design basis events such as nuclear power plant transients and Loss-of-Coolant Accidents (LOCA). MELCOR is an engineering-level computer code that is primarily used to analyze beyond design basis events such as the progression of severe accidents in light water reactor nuclear power plants. Both codes model containment heat transfer and it is important to assess the accuracy of RELAP5 and MELCOR code for condensation in the presence of noncondensable gases. Early work in the simulation of condensation experiments in the presence of noncondensable gases using the RELAP5/MOD3 code was done by Hassan [15]. The code was applied to simulate four different experiments and it was suggested that a new refined heat transfer condensation model in the presence of noncondensable gases was needed. Park [16] improved the standard RELAP5/MOD3.2 code using the non-iterative modeling and several existing condensation correlations of liquid-side heat transfer coefficient, wall friction factors and interfacial friction factors. Aglar [17] assessed the condensation module of RELAP5/MOD3.3 code using experimental works conducted at the Massachusetts Institute of Technology (MIT), the University of California-Berkeley (UCB), and the Middle East Technical University (METU). The results show that the heat transfer coefficients can be predicted by RELAP5/Mode3.3 with the approximate mean deviation of 150%, 85% and 50% for METU, UCB and MIT databases, respectively. Hogan [18] implemented the generalized diffusion layer model into the MELCOR code. Validation work has been conducted to demonstrate the accuracy of the generalized diffusion layer model in MELCOR for condensation with noncondensable gas.

In this paper, the condensation models considering the presence of noncondensable gas of RELAP5-3D code, MELCOR code and the generalized diffusion layer model were examined by Anderson's AP600 containment experiment at atmospheric conditions [4]. The RELAP5-3D code was found may be inaccurate on predicting condensation process with the presence of noncondensable gas. The MELCOR simulation results of AP600 containment experiment were presented in this paper.

2. DESCRIPTION OF SEPARATE EFFECTS AP600 EXPERIMANET

Anderson and coworkers [4] performed experiments for the AP600 using a scaled facility. The main components of Anderson's experiment facility are the test vessel, the coolant system, and the steam supply system. This paper only examines Anderson's "atmospheric tests". The rectangular test vessel represents 1:12 scale radial slices of the AP600 containment from the operating deck to the top of the containment [4].

The test vessel has two 0.91 m long aluminum condensing plates, one oriented vertically and one horizontally, in the top right hand corner of the facility as shown in Fig. 2. Each condensing plate was fitted with six coolant plates, so that the temperature of condensing plate was kept at a fixed value by

cooling each section individually. Coolant water passed through the cooling plates. A mixture of air and water vapor enters the facility from nineteen inlets along the bottom of the test section. The total system pressure remained constant at 1 bar, and the aluminum condensing plates were held at a temperature at approximately 30 °C. This paper simulated four test conditions with different air mass fractions (Table I).

The test section was equipped with several temperature probes as shown in Fig. 2. The probe holes (thermocouple probe 1-7) located in the right hand corner next to the condensing plates were reported as the test temperatures and were used as the bulk mixture temperatures in the calculation of the heat transfer coefficient.

Table I. Steady-state conditions of AP600 containment atmospheric tests

Test	Bulk pressure (bar)	Air mass fraction	Bulk temperature (°C)	Wall temperature (°C)
202	1.0	0.8618	60.65	28.60
203	1.0	0.7900	69.23	29.40
213	1.0	0.6472	79.68	34.00
219	1.0	0.4159	89.72	30.30

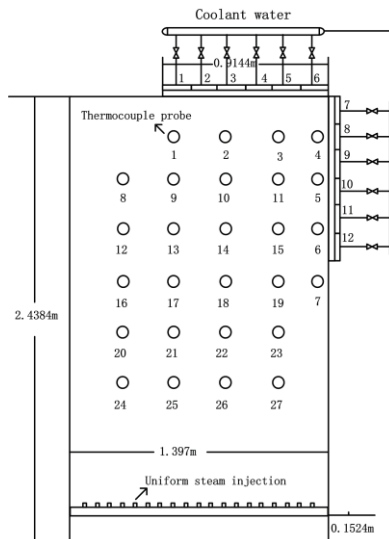


Figure 2. Schematic of Atmospheric Test Section with Cooled Top and Side Walls Shown. Remaining Walls Were Insulated.

Condensation occurred on both the vertical and horizontal plates. Two different methods were used to determine heat transfer coefficient from the experimental data: HEM and CEB. HEM refers to local heat flux measurement. It uses a linear array of thermocouples imbedded in the cooling plates. CEB refers to coolant energy balance, which measures averaged heat transfer coefficient on each individual plate, an energy balance on the coolant water would yield the energy removed from the condensing plate and thus the heat flux associated with the area under the cooling plate could be found. Heat transfer coefficients determined via simulation were compared with those determined by HFM method.

$$h_i = \frac{k(dT_i / dx)}{T_{b,i} - T_{w,i}} \quad (1)$$

where h_i is the heat transfer coefficient of plate i , k is the thermal conductivity of the aluminum plate, dT_i / dx is the temperature gradient through the plate, and $(T_{b,i} - T_{w,i})$ is the difference of temperature between the wall and bulk mixture.

3. CONDENSATION MODELS

3.1. Condensation Models of the Standard RELAP5-3D Code

For inclined surfaces, the RELAP5-3D [19] model uses the maximum of the Nusselt (laminar) and Shah (turbulent) correlations with a diffusion calculation based on the Colburn-Hougen method when noncondensable gases are present. For horizontal surfaces, the model uses the maximum of the Chato (laminar) and Shah (turbulent) correlations with a diffusion calculation based on the Colburn-Haugen method when noncondensable gases are present.

The formulation of Colburn-Hougen model is based on the principle that the amount of heat transferred by condensing vapor to the liquid-vapor/gas interface by diffusing through the noncondensable gas film is equal to the heat transferred through the condensate film. From this energy conservation principle, the interface pressure and interface temperature can be determined by iteration. The heat transfer rate is then calculated. The equations of calculating heat flux due to condensation of vapor mass flux used by RELAP5-3D model are shown in Table II.

3.2. Condensation Models of MELCOR Code

The MELCOR modeling for heat and mass transfer from containment atmosphere to passive structures and components is based on a heat and mass transfer analogy (HMTA), where common heat transfer correlations are used to obtain both sensible energy and, by analogy mass transfer, through temperature and concentration boundary layers [20], respectively. The liquid side heat transfer coefficient is calculated by the thermal conductivity of the liquid and the film thickness [18].

The principal expression for condensation mass flux at a surface exposed to an atmosphere with a significant partial pressure of noncondensable gases is formulated using a mechanistic approach which models the diffusion of a condensable vapor through a gas layer that contains noncondensable gases [21]. The mass transfer coefficient is calculated via a heat-mass transfer analogy by substituting the Schmidt number for the Prandtl number and the Sherwood number for the Nusselt number. The expressions of mass flux and mass transfer coefficient are shown in Table II.

3.3. The Generalized Diffusion Layer Model Code

A generalized diffusion layer model is proposed by Herranz [11]. This model showed good agreement with Anderson's [4] AP600 containment experimental data. In this model, both film and gas resistances to heat transmission have been accounted for by combining them in series to calculate the total heat flux from the atmosphere to the surface. The initial assumptions concerning the heat flux from the gaseous bulk to the condensate are: the negligible influence of radiative mechanism in the total heat transfer; and the parallel coupling of convective and condensing components of heat flux.

$$q_{bw} = h_T(T_b - T_w) = \frac{h_{film}(h_{conv} + h_{cond})}{h_{film} + h_{conv} + h_{cond}}(T_b - T_w) \quad (2)$$

The condensation heat transfer formulation relies on the application of the heat and mass transfer analogy and the Clapeyron equation to express pressure or concentration dependencies in terms of temperatures. The condensation heat transfer coefficient h_{cond} can be written as:

$$h_{cond} = \frac{Sh}{L_c} k_{cond} \quad (3)$$

where k_{cond} is referred to as a condensation conductivity. Equations for calculating k_{cond} are shown in Table II.

Table II . Steady-state conditions of AP600 containment atmospheric tests

	MELCOR	RELAP5	Diffusion Layer model
Condensation heat flux (W/m²)	$q_{cond} = \dot{m} i_{fg}$	$q_{cond} = \dot{m} i_{fg}$	$q_{cond} = h_{cond} \cdot (T_b - T_i)$
Mass flux (kg/s-m²)	$\dot{m} = H_m \rho_v \ln((1 - \frac{P_{vl}}{P}) / (1 - \frac{P_{vb}}{P}))$ ρ_v : density of vapor at $T_{sat}(P_{tot})$	$\dot{m} = H_m \rho_{vb} \ln((1 - \frac{P_{vl}}{P}) / (1 - \frac{P_{vb}}{P}))$ ρ_{vb} : saturation vapor density at P_{vb}	None
Mass transfer coefficient (m/s)	$H_m = Sh \cdot D_m / L_c$	$H_m = \max(H_{mv}, H_{ml}, H_{mn})$ $h_{mn} = Sh \cdot D_m / L_c$	None
Sherwood number	$Sh = Nu \cdot Sc^{1/3} \cdot Pr^{-1/3}$	$Sh = \left[0.825 + \frac{0.387(Ra_{LD})^{1/6}}{\left[1 + \left(\frac{0.492}{Sc} \right)^{9/16} \right]^{8/27}} \right]^2$	$Sh = 0.13 \cdot Gr^{1/3} \cdot Sc^{1/3}$
h_{cond} (W/m²-K)	None	None	$h_{cond} = k_{cond} \cdot Sh \cdot \Theta / L_c$ $k_{cond} = \frac{D_m \cdot i_{fg}^2 \cdot M_v \cdot C}{R_v T_i^2 T_{avg}} \Phi$
Mass diffusivity D_m (m²/s)	$D_m = 0.018583 \frac{[T^3 (\frac{1}{M_v} + \frac{1}{M_n})]^{\frac{1}{2}}}{P \sigma_{vn}^2 \Omega_{D,vn}}$	$D_m = 0.0101325 \frac{(\frac{1}{M_v} + \frac{1}{M_n})^{\frac{1}{2}} T^{1.75}}{P \left[(\varepsilon_v)^{\frac{1}{3}} + (\varepsilon_n)^{\frac{1}{3}} \right]^2}$	$D_m = \frac{[3.03 - (0.98 / M_{v,n}^{1/2})] 10^{-3} T^{3/2}}{PM_{v,n}^{1/2} \sigma_{v,n}^2 \Omega_D}$

3.4. Condensation Heat Fluxes Calculated by Different Models

Condensation heat fluxes due to mass transfer of the four different test conditions in Table I were calculated using the reported gas mixture temperature from each experiment. The expressions of σ , Ω and

ε in mass diffusivity equations can be found in [7] and [22]. The wall temperature was used as the liquid-vapor/gas interface temperature in these calculations. The predicted condensation heat flux with the air mass fraction is shown in Fig. 3. It is necessary to state that the condensation heat fluxes in Fig. 3 are not the simulation results, they are calculated using the equations in Table II through the EES (Engineering Equation Solver) tool. It can be seen that the condensation heat flux decreases with the increasing of air mass fraction. Fig.3 also shows that the RELAP5-3D model underestimated the condensation heat flux due to the modeling of the mass transfer in the gas mixture, and the error increases with increasing air mass fraction.

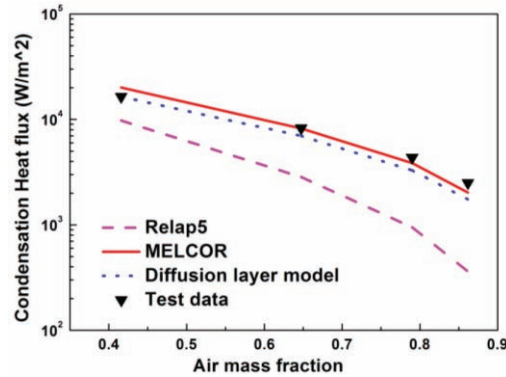


Figure 3. Prediction of Condensation Heat Flux with the Air Mass Fraction. Comparison between Different Condensation Models Using Test Bulk Temperature.

In the process of calculating condensation heat flux, the main difference between MELCOR model and RELAP5 model is that different densities were used when calculating the mass flux. The expression of the mass flux in MELCOR model is equation (4), using the density of vapor at the saturation temperature of total pressure. While the expression of the mass flux in RELAP5 model is equation (5), using the saturation vapor density at vapor partial pressure. The divergence between ρ_v and ρ_{vb} increases with the increase of the air mass fraction.

$$\dot{m} = H_m \rho_v \ln\left(\frac{1 - \frac{P_{vi}}{P}}{1 - \frac{P_{vb}}{P}}\right) \quad (4)$$

$$\dot{m} = H_m \rho_{vb} \ln\left(\frac{1 - \frac{P_{vi}}{P}}{1 - \frac{P_{vb}}{P}}\right) \quad (5)$$

where ρ_v is the density of vapor at $T_{\text{sat}}(P_{\text{tot}})$, ρ_{vb} is the saturation vapor density at P_{vb} .

Following is the derivation of condensation mass flux using the general Fick's law of diffusion to examine which of the two different models is more theoretically appropriate.

3.5. Derivation of the Condensation Heat Flux Due to Mass Transfer

The condensation heat flux is the function of mass flux:

$$q_{\text{cond}} = \dot{m} \cdot i_{fg} \quad (6)$$

where q_{cond} is the condensation heat flux, $W/m^2 \cdot s$. \dot{m} is the mass flux of steam, $kg/m^2 \cdot s$. i_{fg} is the latent heat of vaporization, J/kg .

The mass flux of noncondensable gas at the interface includes the bulk flow and the diffusive component:

$$Cv_{gi} = Cx_{gi}v_i + J_g \quad (7)$$

C is the total molar density, mol/m^3 . v_{gi} is the velocity of noncondensable gas at the interface, m/s . x_{gi} is the mole fraction of noncondensable gas at the interface. v_i is the average bulk flow velocity, m/s . J_g is the diffusive molar flux of noncondensable gas, $mol/m^2 \cdot s$.

According to the Fick's law,

$$J_g = -CD \frac{\partial x_g}{\partial y} \quad (8)$$

$$Cv_{gi} = Cx_{gi}v_i - CD \frac{\partial x_g}{\partial y} \quad (9)$$

Because the interface is impermeable to the noncondensable gas, so the absolute noncondensable gas velocity at the interface equals zero, $v_{gi} = 0$, so the average velocity is

$$v_i = \left(D \frac{1}{x_g} \frac{\partial x_g}{\partial y} \right)_i = \left(D \frac{\partial}{\partial y} \ln(x_g) \right)_i \quad (10)$$

Define δ_g as the effective thickness of the diffusion layer,

$$v_i = \frac{D}{\delta_g} (\ln(x_{gb}) - \ln(x_{gi})) \quad (11)$$

Because $Sh = \frac{L_c}{\delta_g} = \frac{H_m L_c}{D}$, we can get:

$$v_i = H_m (\ln(x_{gb}) - \ln(x_{gi})) \quad (12)$$

The mass flux of steam at the interface is:

$$\begin{aligned} \dot{m} &= -M_v (Cx_{vi}v_i + J_v) \\ &= -M_v (Cx_{vi}v_i + Cx_{gi}v_i) \\ &= -CM_v v_i \end{aligned} \quad (13)$$

Combining the Eq. (12) with Eq. (13), the steam mass flux can be expressed as:

$$\dot{m} = \rho_v H_m \ln\left(\frac{1 - \frac{P_{vi}}{P}}{1 - \frac{P_{vb}}{P}}\right) \quad (14)$$

The mass flux obtained from the above analysis is in agreement with the MELCOR condensation model. The condensation model that RELAP5-3D uses may be inaccurate on predicting condensation process with the presence of noncondensable gas due to its use of ρ_{vb} .

Since the condensation model of MELCOR code is reasonable. The MELCOR code was used to simulate and analyze the AP600 experiments.

4. MELCOR SIMULATIONS OF AP600 EXPERIMENTS

4.1. MELCOR Nodalization

In MELCOR code, the test vessel is represented by control volumes, flow between control volumes by flow path, and condensing plates by heat structures. The back wall temperature of heat structure (outer plate temperature) was fixed as a boundary condition from test data. The steady-state conditions of tests were used as the initial conditions for the simulation. In other words, the simulation only dealt with the steady state of the experiment and transient behavior in the beginning of the experiment was neglected. Steam was injected from the bottom of the vessel. The steam velocity was adjusted to reach the bulk temperature, total pressure and partial pressure of the test conditions. In this work, three different nodalizations (Fig. 4) were studied to analyze the effects of nodalizations. Nodalization (a) used five volumes to simulate the test vessel. One large volume was connected to the vertical and horizontal heat structure. Nodalization (b) used eleven volumes to simulate the test vessel. There were six volumes located adjacent to the seven heat structures, four horizontal heat structures and three vertical heat structures. Nodalization (c) used forty volumes to represent the test vessel, eleven volumes located adjacent to twelve heat structures, six horizontal heat structures and six vertical heat structures. Additional control volumes away from the cooled walls had little effect based on other simulation results.

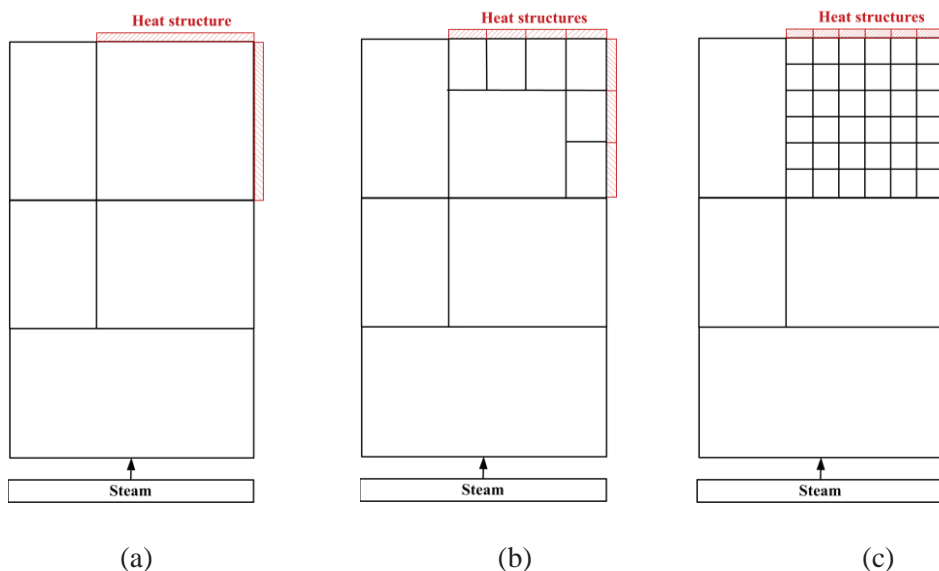


Figure 4. MELCOR Nodalizations of AP600 Containment Test.

4.2. Analysis of Different Nodalizations in MELCOR

According to the experimental test protocol, different bulk temperatures were achieved by increasing the amount of steam injected in the vessel. The state of injection steam is superheated at 1.7 bar and 125.13 °C. Fig. 5 represents the steam injection rate to reach the specific steady state condition. The injection steam mass flow rate decreases with the increasing of air mass fraction. Fig. 5 shows that the steam mass flow rate calculated by the nodalization (c) is larger than that calculated by nodalization (a) and nodalization (b).

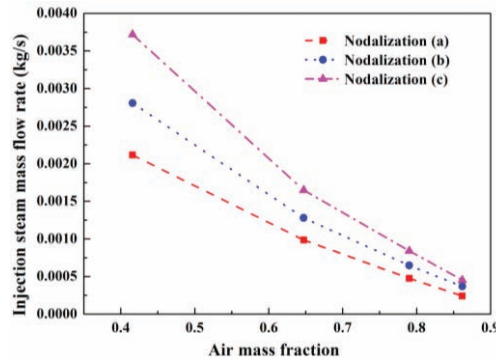


Figure 5. The Mass Flow Rate of Injection Steam versus Air Mass Fraction.

Fig. 6 shows the distribution of film thickness calculated by MELCOR code using different nodalizations for test 202. Although the predicted film thickness is small (20~60 microns), the presence of film still imposes a noticeable effect on the heat transfer. It can be seen that only the nodalization (c) reflects the variation of film thickness with the vertical distance from the top of the test vessel. The film thickness calculated by nodalization (c) increases with the increase of vertical distance. While the film thickness calculated by nodalization (a) and nodalization (b) is almost constant along the vertical direction. Fig. 6 also shows that the film thickness calculated by nodalization with more control volumes is thinner than that calculated by nodalization with fewer control volumes.

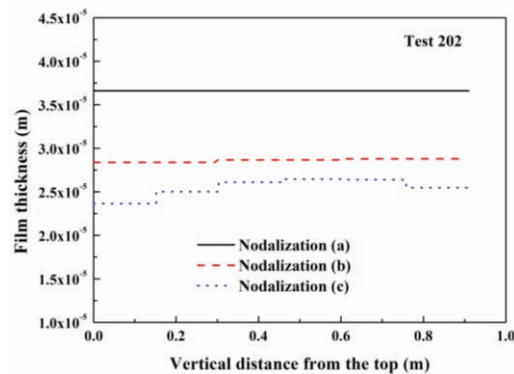


Figure 6. Distribution of Film Thickness Calculated by MELCOR for Test 202.

For a similar reason, the condensation heat flux depends on the mass flux of steam in the diffusion layer. The distributions of mass flux calculated based on three different nodalizations for test 202 were shown in Fig. 7. The mass flux calculated by nodalization (c) is larger than that calculated by other two

nodalizations. And the nodalization (c) calculation can also reflect the distribution of mass flux along the vertical distance from the top. This is because that nodalization (a) and nodalization (b) use the average temperature as the bulk temperature of test condition, while the nodalization (c) uses local temperature as the bulk temperature. Therefore nodalization (c) can predict the temperature stratifications.

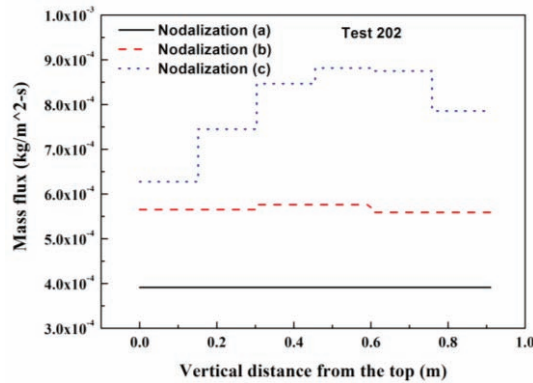


Figure 7. Distribution of Mass Flux Calculated by MELCOR for Test 202.

4.3. Comparison of MELCOR Results with Test Data

The total heat transferred out of the cooled surface calculated using three different nodalizations were compared with test data in Fig. 8. It can be seen that with the increase of air mass fraction, the total heat transfer decreases as expected. For all nodalizations, the deviation from the experimental data increases with the increasing of air mass fraction. As expected, using additional control volumes in MELCOR simulations, improved the simulation results. This can be explained through Fig. 6 and Fig. 7, the film thickness calculated by nodalization (c) is the thinnest one, and the mass flux calculated by nodalization (c) is the largest one. In the test facility, each condensing plates was fixed to six condensation plates, accordingly, nodalization (c) used six vertical heat structures and six horizontal heat structures, which most closely matches to the actual geometric of the test vessel. From Fig. 8 it can be concluded that nodalization (c) best models the experiment. So the following analysis are based on the results of nodalization (c).

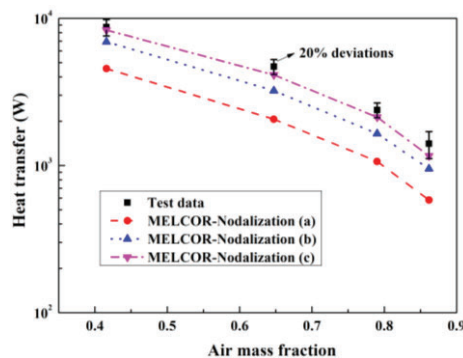


Figure 8. Comparison of MELCOR Code Calculations with Test Data.

The distributions of film thickness for different test conditions were shown in Fig. 9, and the distributions of mass flux for different test conditions were shown in Fig. 10. The air mass fraction of test 219 is the smallest among the four test conditions, leads to the largest film thickness and the highest mass flux.

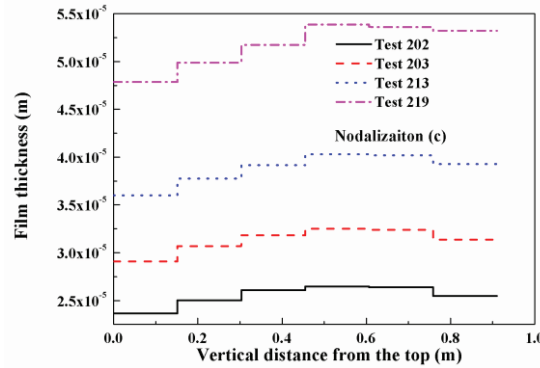


Figure 9. Distribution of Film Thickness Calculated by MELCOR for Four Different Test Conditions.

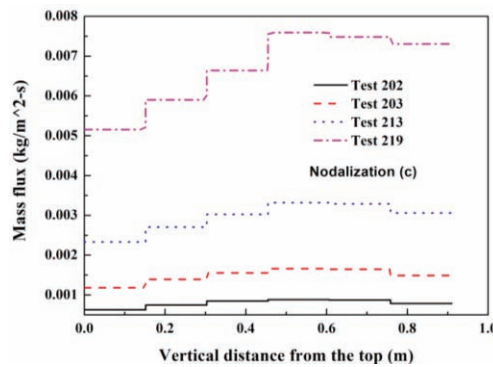


Figure 10. Distribution of Mass Flux Calculated by MELCOR for Four Different Test Conditions.

When noncondensable gas exists, the total thermal resistance from the gas bulk to the condensing plates can be calculated by equation (15). The convection thermal resistance (R_{conv}), the condensation thermal resistance (R_{cond}), the liquid film thermal resistance (R_{film}) and the total thermal resistance (R_{total}) calculated by the nodalization (c) were shown in Fig. 11. It can be seen that with the increase of air mass fraction, the convection resistance, the condensation resistance and the total thermal resistance increase. While the liquid film thermal resistance decreases with the increase of air mass fraction. This is because higher air mass fraction indicates lower steam mass fraction. Lower steam fraction leads to thinner liquid film, which results in a lower film thermal resistance. Fig. 11 also shows that for large air mass fraction, the gas condensation thermal resistance is the main resistance of the system. So the accuracy of calculating the condensation heat flux due to mass flux is the key to the prediction of the total heat transfer.

$$R_{total} = R_{film} + \left(\frac{1}{R_{conv}} + \frac{1}{R_{cond}} \right)^{-1} \quad (15)$$

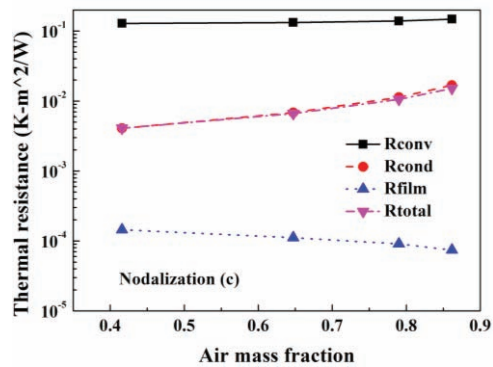


Figure 11. Evolution of Thermal Resistances with the Air Mass Fraction.

5. CONCLUSIONS

The condensation models of MELCOR code and RELAP5 code were analyzed to study the condensation in presence of noncondensable gases. The calculation results were compared to scaled AP600 containment atmospheric experiments by Anderson [4]. The following conclusions are drawn from this study:

- (1) The MELCOR model and RELAP5 model both consider the effect of noncondensable gas, based on the principle that the amount of heat transferred by condensing vapor to the liquid-vapor/gas interface is controlled by diffusion through the noncondensable gas film balanced by the heat transferred through the condensate film. The major difference is that MELCOR and RELAP-3D use different densities to calculate the condensation mass flux. The density of vapor at the saturation temperature of total pressure is used by MELCOR code, whereas RELAP5 uses the saturation vapor density at vapor partial pressure. Based on the derivation of the condensing steam mass flux, the relationship that MELCOR uses is more appropriate with the physical process. The RELAP5 model does not seem to be reliable in predicting the process of condensation with the significant presence of noncondensable gas.
- (2) The MELCOR code can be used to predict the heat transfer in the presence of noncondensable gases. MELCOR simulations showed good agreement with AP600 experimental data. But nodalization is important for the simulation, as different nodalizations can lead to significant different results. The nodalization should closely match to the actual geometric of the test vessel.
- (3) The total thermal resistance between the gas bulk and the condensing wall consists of the different thermal resistances from convection, condensation and liquid film. At the atmospheric condition, when the air mass fraction is relatively large (0.4~0.9), the condensation thermal resistance is the major thermal resistance of the condensing system. The condensation film resistance is a second order effect.

REFERENCES

1. H. Uchida, A. Oyama, and Y. Togo, *Evaluation of Post-incident Cooling Systems of Light Water Power Reactors*, Tokyo University, Tokyo, Japan (1964).
2. T. Tagami, *Interim Report on Safety Assessments and Facilities Establishment Project for June 1965, No.1*. Japanese Atomic Energy Research Agency (1965), unpublished work.

3. A.A. Dehbi, *The Effects of Noncondensable Gases on Steam Condensation under Turbulent Natural Convection Conditions*, Massachusetts Institute of Technology, USA (1991).
4. M.H. Anderson, L.E. Herranz, and M.L. Corradini, "Experimental Analysis of Heat Transfer within the AP600 Containment under Postulated Accident Conditions," *Nuclear Engineering and Design*, **185**(2), pp. 153-172 (1998).
5. A.P. Colburn and O.A. Hougen, "Design of Cooler Condensers for Mixtures of Vapors with Noncondensing Gases," *Industrial & Engineering Chemistry*, **26**(11), pp. 1178-1182 (1934).
6. M.L. Corradini, "Turbulent Condensation on a Cold Wall in the Presence of a Noncondensable Gas," *Nuclear Technology*, **64**(2), pp. 186-195 (1983).
7. R.B. Bird, W.E. Stewart, and E.N. Lightfoot, *Transport Phenomena*, John Wiley & Sons, New York, USA (2007).
8. M.H. Kim and M.L. Corradini, "Modeling of Condensation Heat Transfer in a Reactor Containment," *Nuclear Engineering and Design*, **118**(2), pp. 193-212 (1990).
9. P.F. Peterson, V.E. Schrock, and T. Kageyama, "Diffusion Layer Theory for Turbulent Vapor Condensation with Noncondensable Gases," *Journal of Heat Transfer*, **115**(4), pp. 998-1003 (1993).
10. H.J.H. Brouwers, "Effect of Fog Formation on Turbulent Vapor Condensation with Noncondensable Gases," *Journal of Heat Transfer*, **118**(1), pp. 243-245 (1996).
11. L.E. Herranz, M.H. Anderson, and M.L. Corradini, "A diffusion Layer Model for Steam Condensation within the AP600 Containment," *Nuclear Engineering and Design*, **183**(1), pp. 133-150 (1998).
12. P.F. Peterson, "Diffusion Layer Modeling for Condensation with Multicomponent Noncondensable Gases," *Journal of Heat Transfer*, **122**(4), pp. 716-720 (2000).
13. Y. Liao and K. Vierow, "A Generalized Diffusion Layer Model for Condensation of Vapor with Noncondensable Gases," *Journal of Heat Transfer*, **129**(8), pp. 988-994 (2007).
14. J.W. Kim, Y.G. Lee, H.K. Ahn, et al., "Condensation Heat Transfer Characteristic in the Presence of Noncondensable Gas on Natural Convection at High Pressure," *Nuclear Engineering and Design*, **239**(4), pp. 688-698 (2009).
15. Y.A. Hassan and L.L. Raja, "Analysis of Experiments for Steam Condensation in the Presence of Non-condensable Gases Using the RELAP5/MOD3 Code," *Nuclear Technology*, **104**(1), pp. 76-88 (1993).
16. H.S. Park, H.C. No, and Y.S. Bang, "Analysis of Experiments for In-tube Steam Condensation in the Presence of Noncondensable Gases at a Low Pressure Using the RELAP5/MOD3. 2 Code Modified with a Non-iterative Condensation Model," *Nuclear Engineering and Design*, **225**(2), pp. 173-190 (2003).
17. F. Ađlar, "Assessment of the RELAP5/MOD3. 3 Code for Condensation in the Presence of Air Using Experimental Data and Theoretical Model," *Annals of Nuclear Energy*, **60**, pp. 329-340 (2013).
18. K. Hogan, Y. Liao, B. Beeny, et al., "Implementation of a Generalized Diffusion Layer Model for Condensation into MELCOR," *Nuclear Engineering and Design*, **240**(10), pp. 3202-3208 (2010).
19. C. Fletcher and R. Schultz, *RELAP5-3D Code Manual Volume IV: Models and Correlations*, Idaho, National Engineering Laboratory, Lockheed Idaho Technologies Company, Idaho Falls, Idaho (2005).
20. J. Tills, A. Notafrancesco, and L. Pamela, *An Assessment of MELCOR 1.8.6: Virginia Tube Reactor (CVTR) Containment (Including Selected Separate Effects Tests)*, Sandia National Laboratories, USA (2008).
21. R.O. Gauntt, R.K. Cole, C.M. Erickson, et al., *MELCOR Computer Code Manuals Vol. 2: Reference Manuals*, NUREG/CR-6119 (2010).
22. A.F. Mills, *Mass Transfer*, Vol. 2, Prentice Hall Upper Saddle River, NJ, USA (2001).